Parallel Link-based Light-Weight Leg Design for Bipedal Robots

Yuichi Tazaki†

***Abstract*— A new leg design for bipedal walking robots that utilizes 6-dof parallel link mechanism is proposed. Reducing leg inertia is a crucial requirement for realizing agile walking and fall avoidance involving multiple stepping. The proposed parallel link design enables embedding all leg actuators in the torso and thereby significantly reducing the leg inertia. Some fundamental kinematic characteristics of the proposed leg mechanism including movable range and maximum static load is shown. A real small-sized humanoid robot equipped with the proposed leg mechanism is developed. Experimental results show that the proposed leg mechanism achieves high position tracking performance even at high frequencies, and that the robot is able to perform basic walking maneuvers with different strides and step durations.**

I. Introduction

Humanoid robots are expected to perform various tasks in human-living environment by utilizing its morphological similarity to human being. In order for humanoid robots to support humans without disturbing them or risking their safety, humanoid robot must be able to avoid falling and maintain balance against various disturbances. Active fall-avoidance control has been extensively studied in the past decade [1][2][3][4]. In particular, capturability-based analysis has been established as a theoretical framework for discussing fall-avoidance strategy involving multiple footsteps, which is required to cope with strong disturbances. As pointed out in [2], however, N-step strategy with $N \geq 2$ requires very small step duration (about 0.3[s]). Most of today's humanoid robots have serial link legs, for which high-power actuators are needed for driving large inertia of the legs at high speed.

For industrial robots, on the other hand, parallel mechanisms have been widely used for the design of robotic manipulators with small inertia that can be used for tasks such as fast object picking. It is therefore quite natural to think that parallel links can also be used for the leg mechanism of bipedal robots. There are a number of existing studies that utilize parallel mechanisms, either partially or entirely, in the leg design of bipedal walking robots. Some recently developed humanoid robots such as Atlas [5] and RHP2 [6] use parallel links as intermediate links for driving rotational joints by hydraulic/electric cylindrical actuators. In the design of the Cassie robot, parallel link is used for driving knees and ankles via high-power motors placed near the torso [7]. For small-sized humanoid robots actuated by low-cost servo motors, it is a common practice to design the legs as parallel links and drive each joint with multiple servo motors [8].

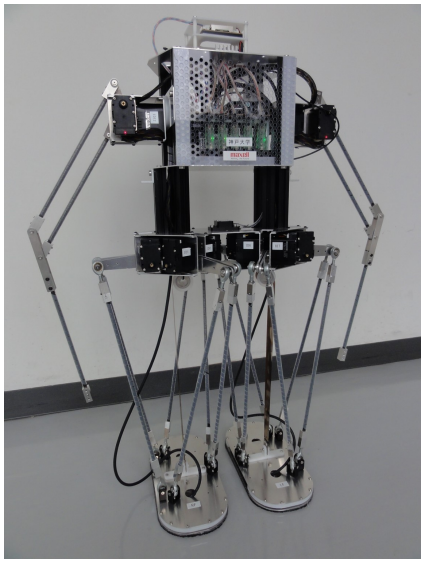

Fig. 1. Photo of the developed bipedal robot

There are also a number of studies in which parallel mechanism is more aggressively used in the entire leg design. Sugawara et al developed a bipedal locomotor WL-16 whose legs are driven by 6-axis parallel platform [9]. Their primary motivation for using parallel mechanism seems to be achieving large payload. Moreover, cylindrical actuators based on ball-screw is not suited to size reduction, so adopting their mechanism for small-sized humanoid robots seems difficult. The leg mechanism of the Atrias robot is configured as planar parallel link, and the longitudinal and vertical movement of the foot is driven by two motors attached near the base link [10][11]. This robot is reported to walk successfully on uneven terrain, but it seems to have poor performance in turning. Gim et al proposed a leg mechanism in which a pair of planar five-bar linkages are connected together at the end [12]. The kinematic study of this mechanism is limited to translational motion, and rotational movable range is not made clear.

In this research, a new parallel link-based leg design that can realize bipedal robots with small leg inertia is proposed. The proposed design uses rotational joints as the actuated joints, and therefore it enables low-cost and small-sized design using off-the-shelf servo motors. Moreover, in contrast to cylindrical actuator-based design, all rotational actuators can be embedded in the torso of the robot, which

†The author is with Faculty of Engineering, Department of Mechanical Engineering, University of Kobe, 1-1 Rokkodai, Nada-ku, Kobe, Japan. tazaki@mech.kobe-u.ac.jp

TABLE I

SPECIFICATION OF THE DEVELOPED ROBOT

Total mass	7.2[kg]
Torso mass	5.5[kg]
Foot mass	0.33[kg]
Max. walking speed	0.3[m/s]
Operational period	90[min]

TABLE II

ROTAIONAL MOVABLE RANGE IN [RAD]([DEG])

	minimum	maximum
roll	-0.25 (-14)	$+0.25$ ($+14$)
pitch	-0.45 (-25)	$+0.30$ ($+17$)
yaw	-0.80 (-45)	$+0.80$ ($+45$)

dramatically reduces the leg inertia. A small-sized humanoid robot that is equipped with the proposed leg mechanism is developed, and its basic walking performance is evaluated.

The rest of this paper is organized as follows. The overview of the developed humanoid robot is provided in Section II. The results of kinematic analysis of the proposed leg mechanism is presented in Section III. Brief description of the hardware and controller architecture of the developed robot is provided in Section IV. Experimental results of position-tracking performance test of the leg mechanism and walking test of the robot are shown in Section V. Concluding remarks are given in Section VI. Throughout the paper, the x, y, and z axis are defined as the longitudinal, lateral, and vertial direction with respect to the robot, and roll, pitch, and yaw are defined as rotations along the x, y, and z axis, respectively.

II. OVERVIEW OF THE DEVELOPED ROBOT

The developed bipedal robot with parallel leg mechanism is shown in Fig. 1, and its main specification is summarized in Table I. Roughly 76% of the whole mass is concentrated around the torso. Each leg is driven by 6-axis parallel mechanism, in which all six rotational actuators are installed in the base link (i.e., the torso), and the rotational movement of the actuators are transferred to the foot via the input links and the rods. Each leg, which consists of six units of input links and rods and a foot, weighs 0.8[kg], while the foot alone weighs 0.33[kg] including the embedded 6-axis force sensor, which is only 5% of the whole weight. This high torso-to-foot mass ratio enables agile foot movement with low torque actuators. It also makes controlling the robot much easier because the influence of the leg inertia to the whole-body dynamics becomes negligible.

III. KINEMATIC ANALYSIS

A. Brief description of the proposed mechanism

The illustrative drawings of four similar parallel mechanisms are shown in Figs. 2(a)-(d), in which the proposed one is shown in Fig. 2(a). In the figure, the upper part is the base link, which is connected to the torso, whereas the lower part

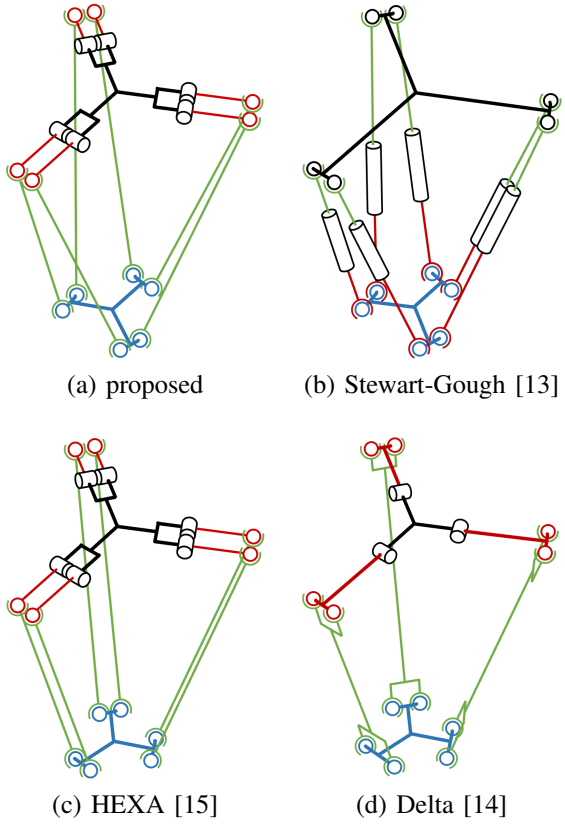

(a) proposed (b) Stewart-Gough [13]

(c) HEXA [15] (d) Delta [14]

Fig. 2. Illustrative drawings of similar parallel mechanisms

is the end link, which is connected to the foot. There are six actuated rotational joints on the base link. Two parallel joints form a pair, and three pairs are installed to form a triangle. An input link is connected to each actuated joint, and the end of each input link is connected to one end of a rod with a spherical joint. The other end of each rod is connected to the corresponding spherical joint attached to the end link. The six spherical joints on the end link are also configured to form a triangle. The mechanism adopted in our leg design can be seen as a close variant of the Hexa robot [15]. It is also widely known as 6-RSS (Rotational-Spherical-Spherical) parallel manipulator [16]. There is one subtle but critical difference between the proposed mechanism and the Hexa robot; in Hexa, the adjacent rods are configured exactly parallel to each other resembling the Delta robot [14], whereas in our mechanism, the rods are configured to form triangles just like the Steward-Gough platform [13]. The former configuration results in very poor manipulability in the yaw rotation (rotation along the vertical axis). The proposed configuration significantly improves both the movable range and the manipulability of yaw rotation. It [16], similar design was synthesized by optimizing the kinematic parameters of 6-RSS manipulators.

B. Analytical Solution of Inverse Kinematics

The inverse kinematics of 6-RSS parallel mechanism can be solved analytically. It has already been derived in the past studies such as [16]; we show it here for the reader's

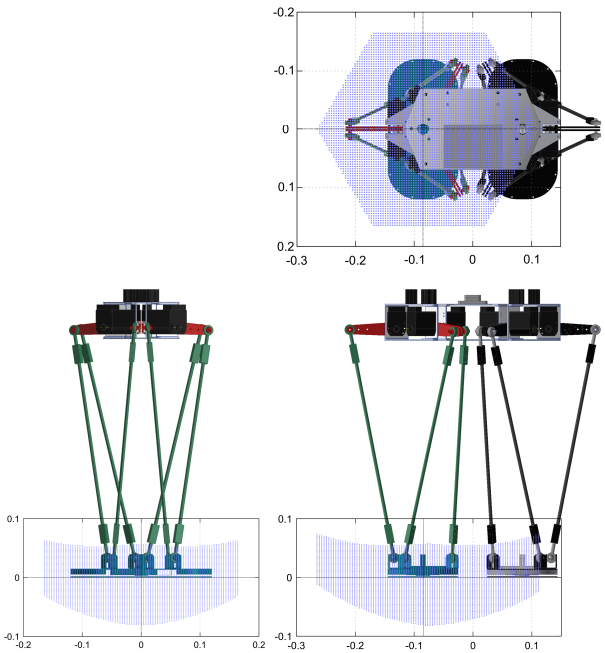

Fig. 3. Translational movable range

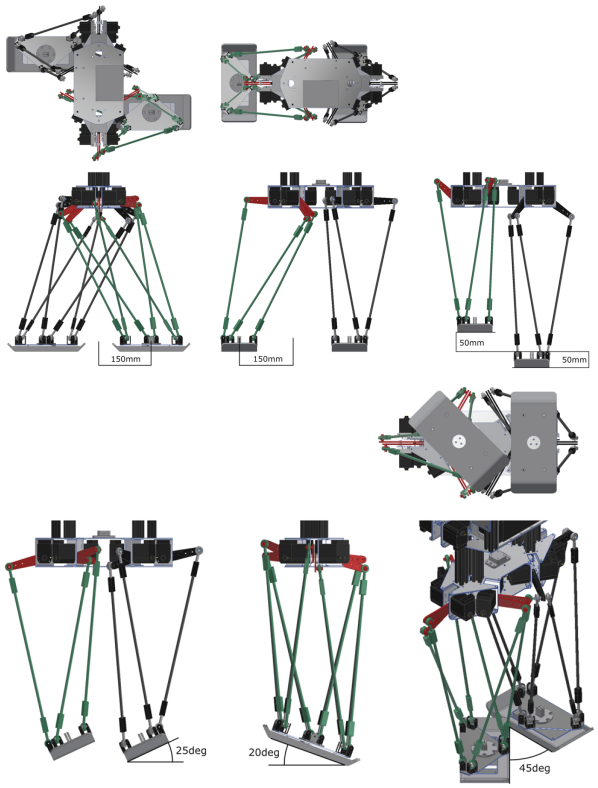

Fig. 4. Postures near movable range limits.

TABLE III

JACOBI MATRIX J AND ITS INVERSE J^{-1} OF THE RIGHT LEG IN THE NEUTRAL POSE

(a) J

	1	2	3	4	5	6
x	+0.109	+0.033	-0.048	+0.048	-0.033	-0.109
y	+0.008	-0.091	+0.082	+0.082	-0.091	+0.008
z	+0.011	+0.004	+0.008	+0.008	+0.004	+0.011
roll	-0.276	+0.128	+0.147	+0.147	+0.128	-0.276
pitch	-0.031	-0.223	-0.254	+0.254	+0.223	+0.031
yaw	+0.831	-0.834	+0.828	-0.828	+0.834	-0.831

(b) J^{-1}

	x	y	z	roll	pitch	yaw
1	+3.316	-0.377	+19.971	-0.985	-0.103	+0.161
2	+1.545	-3.441	+19.893	+0.726	-1.089	-0.244
3	-1.770	+2.302	+20.042	+0.911	-0.993	+0.194
4	+1.770	+2.302	+20.042	+0.911	+0.993	-0.194
5	-1.545	-3.441	+19.893	+0.726	+1.089	+0.244
6	-3.316	-0.377	+19.971	-0.985	+0.103	-0.161

TABLE IV

THEORETICAL MAXIMUM STATIC LOAD OF ONE FOOT (MAXIMUM ACTUATOR TORQUE IS ASSUMED TO BE 4.0[NM])

x	36.0	[N]
y	43.0	[N]
z	363.0	[N]
roll	14.0	[Nm]
pitch	16.0	[Nm]
yaw	4.8	[Nm]

convenience. Given a desired pose of each foot, the desired angle of each joint can be derived separately. Consider a base coordinate frame attached to the center of the base link, and a joint coordinate frame that is attached to the focused joint. Here, the z-axis of the joint coordinate frame matches the rotation axis of the joint. Let $\boldsymbol{p}$, R be the relative translation and rotation of the joint coordinate frame with respect to the base coordinate frame. Moreover, let r denote the length of the input link, and z denote the offset from the end of the input link to the center of the spherical joint. Furthermore, let d be the length of the rod. Since the desired pose of the foot is given, the position of the spherical joint attached to the foot, denoted by $\boldsymbol{q}$, is also known. The kinematic relationship requires that the following equation must hold.

$$\left\| \boldsymbol{p} + R \begin{bmatrix} r\cos\theta \\ r\sin\theta \\ z \end{bmatrix} - \boldsymbol{q} \right\|^2 = d^2. \tag{1}$$

Arranging this equation gives

$$\|\boldsymbol{p}-\boldsymbol{q}\|^2 + r^2 + z^2 + 2(R^\mathsf{T}(\boldsymbol{p}-\boldsymbol{q}))^\mathsf{T} \begin{bmatrix} r\cos\theta \\ r\sin\theta \\ z \end{bmatrix} = d^2. \tag{2}$$

Defining $\hat{\boldsymbol{p}} = R^\mathsf{T}(\boldsymbol{p}-\boldsymbol{q})$, we obtain

$$\begin{bmatrix} \hat{p}_\mathrm{x} \\ \hat{p}_\mathrm{y} \end{bmatrix}^\mathsf{T} \begin{bmatrix} \cos\theta \\ \sin\theta \end{bmatrix} = \frac{d^2 - r^2 - z^2 - 2\hat{p}_\mathrm{z} z - \|\hat{\boldsymbol{p}}\|^2}{2r} := C. \tag{3}$$

Moreover, let us define

$$\gamma = \sqrt{\hat{p}_\mathrm{x}^2 + \hat{p}_\mathrm{y}^2}, \quad \beta = \mathrm{atan2}(\hat{p}_\mathrm{y}, \hat{p}_\mathrm{x}) \tag{4}$$

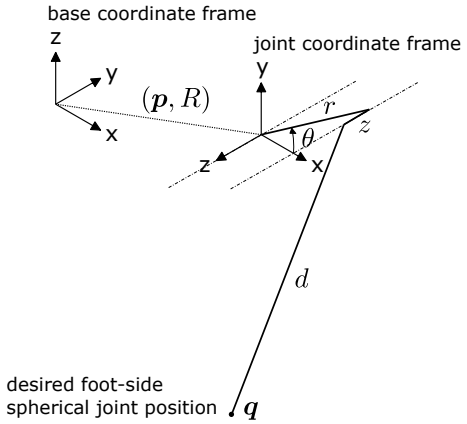

Fig. 5. Inverse Kinematics

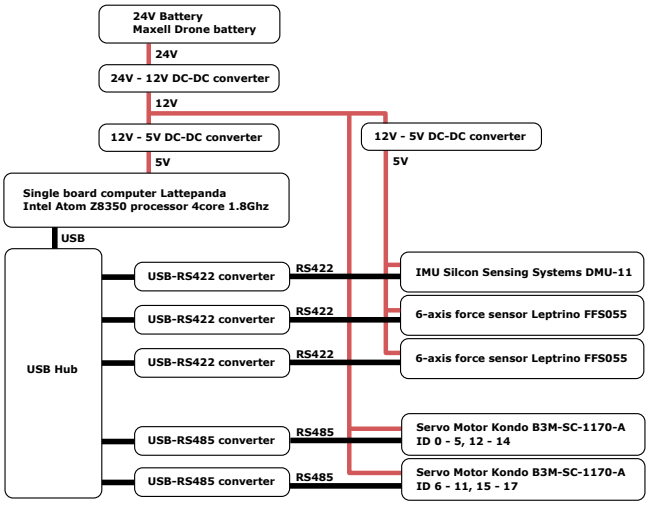

Fig. 6. Hardware Connection

then we get

$$\gamma \cos(\theta - \beta) = C, \quad \theta = \beta \pm \cos^{-1} \frac{C}{\gamma} \tag{5}$$

Among two possible solutions given by $\cos^{-1}$, the one which is inside the valid range of the joint is selected. Infeasibility can be detected by simply checking if C/γ is outside the range $[-1, 1]$.

C. Movable Range

The translational and rotational movable range of the right foot with respect to the torso is shown in Fig. 3, while some postures near the limit of the movable range are illustrated in Fig. 4. Small square markers in each figure indicates a point the center of the foot can reach. The limiting factors of the movable range are the length of the input link r, the length of the rod d, and the maximum tilt angle of the ball joint ($\alpha = 30$[deg]).

The figures show that the movable range in the vertical (z) direction is approximately ± 50[mm], which is sufficient for walking on mild terrain, but not enough for stepping over large obstacles and climbing stairs. The vertical movable range is determined almost solely by the length of the input link r, which is set as 80[mm] in our current design. In order to increase the vertical range, one needs to lengthen the input link. But extending the input link alone clearly increases the load torque, so the length of the input link and the gear ratio of the actuator must be taken into account at the same time.

The longitudinal and lateral (x and y) movable ranges are approximately ± 150[mm], which indicates that theoretically the robot can walk with 300[mm] stride. The longitudinal/lateral movable range is not strongly affected by r, but rather by d and α. This indicates that longitudinal/lateral movable range can be increased by extending the rods or selecting ball joints with wider tilt angle range.

Rotational movable ranges are summarized in Table II. The table shows the minimum and maximum angles the foot can rotate from its neutral posture in each of roll/pitch/yaw directions. The roll/pitch rotation range is wide enough for balance control and walking on a mild slope. The yaw range is more than ± 50[deg], which is large enough for making steep turns. Theoretically, 90deg turn can be achieved in only two steps.

The differential kinematics analysis based on the Jacobian matrix is discussed. The components of the Jacobian matrix of the right foot in its neutral pose is shown in Table III. More concretely, the Jacobian matrix is a 6×6 matrix that maps the joint velocity vector to a 6 dimensional vector consisting of the translational velocity and the angular velocity of the foot. The unit of translation is [m], whereas the unit of rotation is [rad]. It is clear from the table that the Jacobian matrix is a dense matrix, reflecting the characteristics of the parallel mechanism. Let $\boldsymbol{f}$ be the 6-dimensional force vector that expresses the static external load applied to the foot. Then the joint torque vector $\boldsymbol{\tau}$ is given by $\boldsymbol{\tau} = J^{\mathsf{T}} \boldsymbol{f}$. Moreover, consider the case where the external load is exerted in the direction of one specific axis, that is, $\boldsymbol{f}$ is given by $\boldsymbol{f} = \boldsymbol{e}_i f$, where $\boldsymbol{e}_i$ is the unit vector in the i-th direction and f is a scalar. In this case, $\boldsymbol{\tau} = J_{\mathrm{row},i} f$. Let $\tau_{\max}$ be the maximum torque of the actuators. Then the maximum allowable load in the i-th direction is given by

$$f_{\max,i} = \min_j \frac{\tau_{\max}}{J_{i,j}} \tag{6}$$

The maximum continuous torque of the servo motor that is used in our robot is 4[Nm]. The maximum static load in each direction calculated from (6) with $\tau_{\max} = 4.0$ is shown in Table IV. The table shows that the maximum vertical (z-direction) load is remarkably large; three times the robot's own weight can be supported by single foot. The maximum lateral (x and y direction) load, on the other hand, shows relatively small value, approximately half the robot weight. The maximum roll/pitch moment is large enough for balance control. The maximum yaw moment is much smaller than the other two rotational directions.

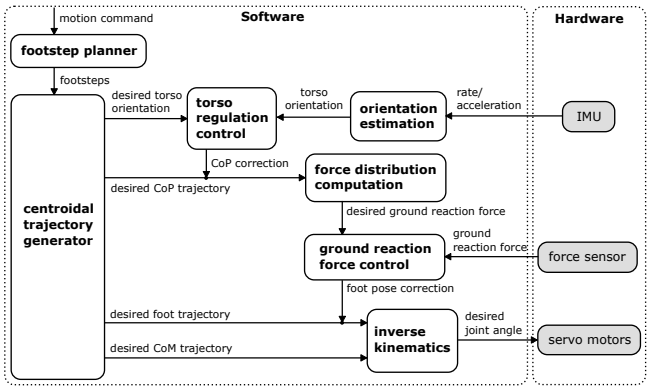

Fig. 7. Controller Design

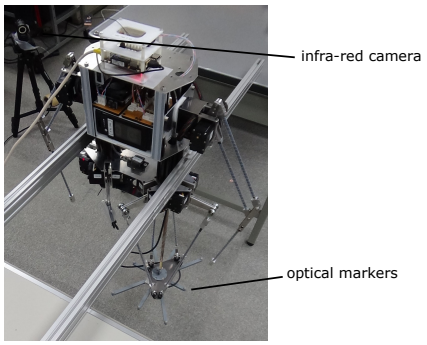

Fig. 8. Experimental setup of foot movement measurement. Four infra-red cameras are installed around the robot. Optical markers are attached to the foot. The left foot is removed to avoid obstructing the camera view.

TABLE V
PARAMETERS OF WALKING MANEUVER

	short stride	long stride
single support period[s]	0.35	0.60
double support period[s]	0.15	0.40
forward stride[m]	0.15	0.25
sideways stride[m]	0.05	0.10
turning angle[deg]	15.0	0.15
lateral foot spacing[m]	0.16	0.16
foot swing height[m]	0.03	0.03

IV. Control System Design and Implementation

This section briefly describes the hardware architecture and the controller design of the developed robot. The hardware connection is illustrated in Fig. 6. The communication bus for the IMU and 6-axis force sensors is RS422, while that of the servo motors is RS485. Each of these serial buses are converted to USB and connected to a USB hub, which is further connected to a single board computer. The output of the 24V battery is converted to 12V and 5V via DC-DC converters and provided to the devices.

The block diagram of the locomotion controller is shown in Fig. 7. The control architecture is a conventional one that has been used in many humanoid robots. Movement command (longitudinal/lateral speed and turning speed) is provided by a high-level navigation controller or a human operator with some input device. The footstep planner determines the next foot placement based on this movement command. Next, the centroidal trajectory generator computes valid center-of-mass trajectory and zero-moment-point trajectory that are consistent with the linear inverted pendulum mode. The orientation controller computes the inclination angles of the torso from the IMU measurement, and determines the amount of correction of the desired ZMP to maintain the torso in the upright posture. The ground reaction force controller converts the desired ZMP to the desired distribution of ground reaction forces, and it then adds correction terms to the desired position and rotation of the feet that compensates the error between the desired reaction forces and the measured forces retrieved from the force sensors. In the final stage, the desired joint angles are computed by solving inverse kinematics. First, the desired torso position is calculated from the desired position/rotation of the feet and the desired CoM position. For simplifying this calculation, the mass of the legs and the arms are neglected. This approximation is acceptable because in our design the legs and arms are mostly composed of CFRP rods. Once the desired torso position is determined, the desired angle of each joint can be calculated analytically as described in Section III-B. The whole control procedure requires very low computational cost and therefore it can be executed on an embedded computer at high enough update rate. In our implementation, the control period is set as 2[ms].

V. Experimental Results

For evaluating the trajectory-tracking performance of the leg, sinusoidal signal was input to each of the six directions of the desired position (x, y, and z) and rotation angle (roll, pitch, and yaw) of the foot while the torso of the robot was fixated to a frame. The frequency of the sinusoidal signal was varied continuously from 0.5[Hz] to 2.0[Hz] over the period of 10 seconds. The amplitude of the signal was set to 0.05[m] for x and y, 0.03[m] for z, and 15[deg] for all rotational directions. The motion of the foot was measured by using a motion capture system. The experimental setup is shown in Fig. 8.

The results are shown in Fig. 9. It is observed in the figure that the leg controller showed generally good performance in all six directions. Slight overshoot is observed in the x and y directions at high frequencies, while in the z direction such overshoot is not observed. As discussed previously, the maximum static load in the x and y directions are much smaller than that in the z direction (see Table IV). For this reason, as the inertial force of the foot becomes greater at higher frequencies, position control error of the servo motors become more evident. Another issue is that constant oscillation in the yaw direction is observed. It is considered that the elastic element (elasticity of the CFRP rod, P-gain of the servo motor) and the inertial element (foot inertia, rotor inertia of the servo motor) contribute to creating a resonance frequency that is slightly below 10[Hz].

The performance of three basic walking maneuvers (forward walking, sideways walking, and turning) in two different levels of stride length was tested. The walking speed is

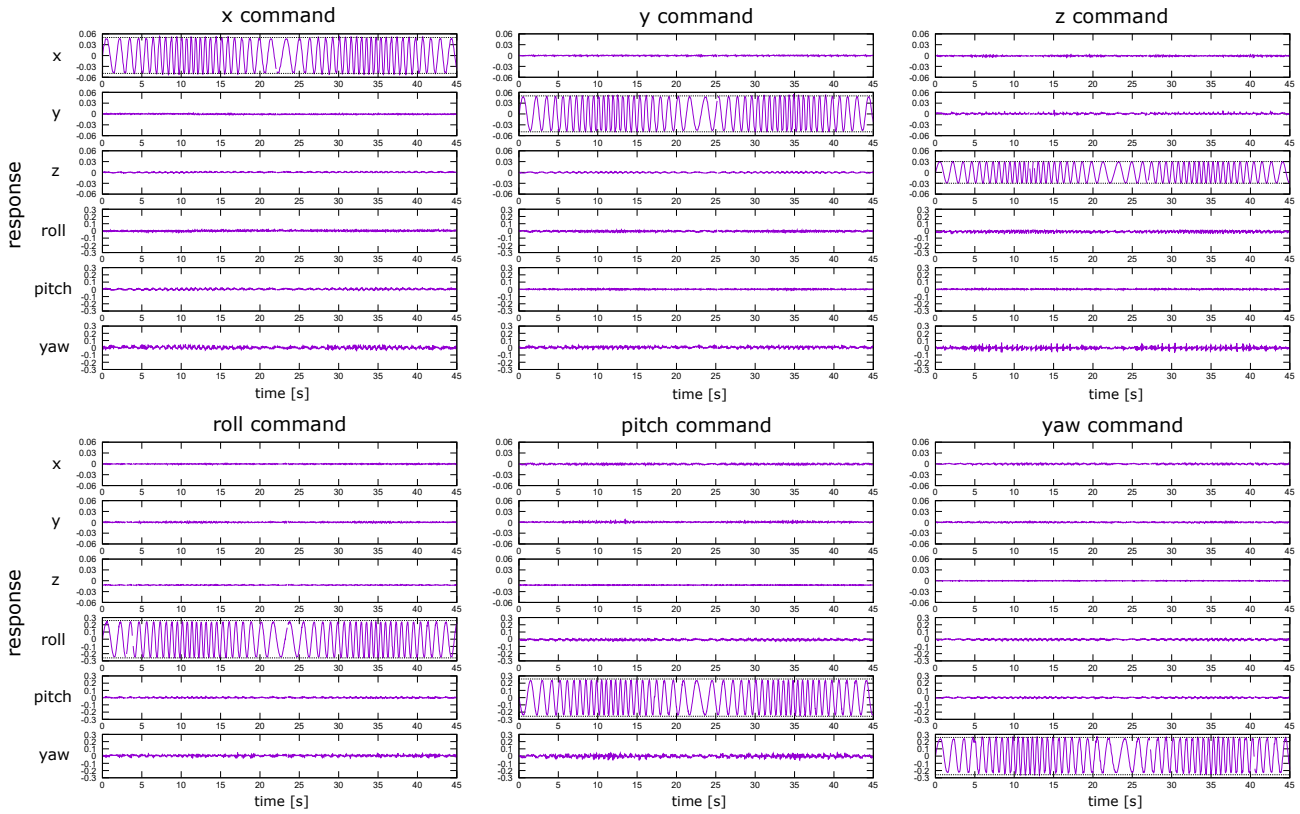

Fig. 9. Motion capture data of foot movement

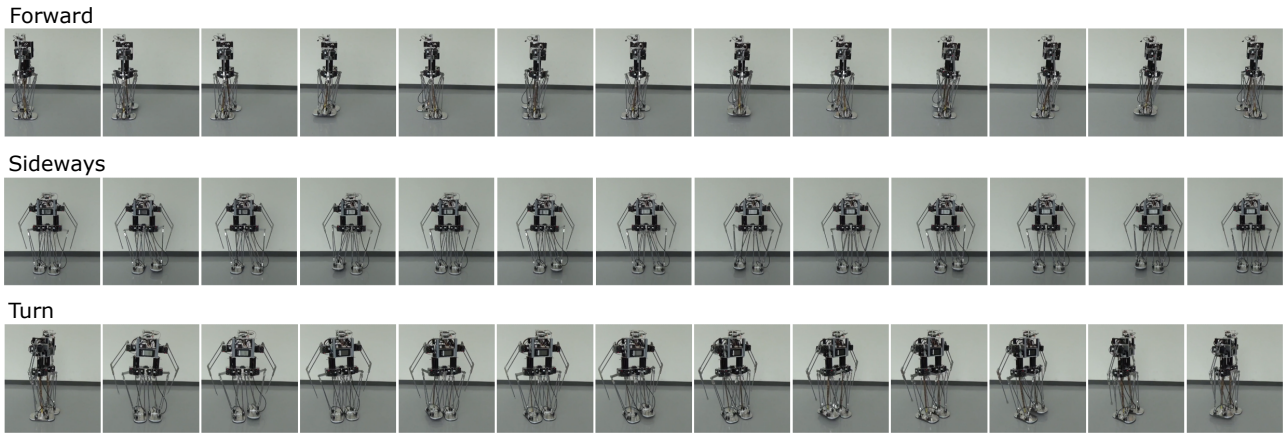

Fig. 10. Snapshots of basic movements

0.3[m/s] in the short stride setting, and 0.25[m/s] in the long stride setting. The robot was able to perform these maneuvers in both settings. In the short stride setting, the robot could move its foot to the desired landing point in only 0.35[s]. This indicates that the robot is suitable for an experiment platform for capturability-based fall avoidance controllers. The snapshots of basic walking movements are shown in Fig. 10. Please also see the attached video.

VI. Conclusion

This paper presented a new parallel link-based leg design for bipedal robots. The proposed design is suitable for realizing quick stepping motion that is required in capturability-based fall avoidance control. One inherent drawback of parallel link compared serial link is its limited movable range. Our ongoing work includes extending the movable range of the proposed leg mechanism in order to improve the mobility of the robot.

ACKNOWLEDGMENT

This research was supported by NSK Foundation for Advancement of Mechatronics.

REFERENCES

[1] B.J. Stephens and C.G. Atkeson: "Push Recovery by Stepping for Humanoid Robots with Force Controlled Joints", IEEE-RAS International Conference on Humanoid Robots, pp.52-59, 2010.

[2] J. Pratt et al.: "Capturability-based Analysis and Control of Legged Locomotion, Part 2: Application to M2V2, a Lower-Body Humanoid", The International Journal of Robotics Research, Vol.31, No.10, pp.1117-1133, 2012.

[3] R.J. Griffin, G. Wiedebach, S. Bertrand, A. Leonessa and J. Pratt: "Walking Stabilization Using Step Timing and Location Adjustment on the Humanoid Robot, Atlas", IEEE/RSJ International Conference on Intelligent Robots and Systems, pp.667-673, 2017.

[4] T. Kamioka et al.: "Dynamic Gait Transition between Walking, Running and Hopping for Push Recovery", IEEE-RAS International Conference on Humanoid Robotics, pp.1-8, 2017.

[5] S. Feng, E. Whitman, X. Xinjilefu, C. G. Atkeson: "Optimization Based Full Body Control for the Atlas Robot", IEEE-RAS International Conference on Humanoid Robots, pp.120-127, 2014.

[6] Y. Kakiuchi, M. Kamon, N. Shimomura, S. Yukizaki, N. Takasugi, S. Nozawa, K. Okada, M. Inaba: "Development of Life-Sized Humanoid Robot Platform with Robustness for Falling Down, Long Time Working and Error Occurrence", 2017 IEEE/RSJ International Conference on Intelligent Robots and Systems (IROS), pp.689-696, 2017.

[7] Z. Xie, G. Berseth, P. Clary, J. Hurst, M. van de Panne: "Feedback Control For Cassie With Deep Reinforcement Learning", IEEE/RSJ International Conference on Intelligent Robots and Systems, pp.1241-1246, 2018.

[8] G. Ficht, H. Farazi, A. Brandenburger, D. Rodriguez, D. Pavlichenko, P. Allgeuer, M. Hosseini, S. Behnke: "NimbRo-OP2X: Adult-sized Open-source 3D Printed Humanoid Robot", 2018 IEEE-RAS 18th International Conference on Humanoid Robots (Humanoids), pp.747-754, 2018.

[9] Y. Sugahara, et al., "Development of a Biped Locomotor with the Double Stage Linear Actuator", Proceedings 2007 IEEE International Conference on Robotics and Automation, pp.1850-1855, 2007.

[10] J.A. Grimes, J.W. Hurst: "The Design of Atrias 1.0 A Unique Monopod, Hopping Robot", Adaptive Mobile Robotics, pp.548-554, 2012.

[11] A. Ramezani, J.W. Hurst, K.A. Hamed, J.W. Grizzle: "Performance Analysis and Feedback Control of ATRIAS, A Three-Dimensional Bipedal Robot", Journal of Dynamic Systems, Measurement, and Control, Vol.136, No.2, 2013.

[12] K.G. Gim, J. Kim and K. Yamane: "Design of a Serial-Parallel Hybrid Leg for a Humanoid Robot", 2018 IEEE International Conference on Robotics and Automation (ICRA), pp.1-5, 2018.

[13] D. Stewart: "A Platform with Six Degrees of Freedom", Proceedings of the Institution of Mechanical Engineers, Vol.180, No.1, pp.371-386, 1965.

[14] F. Pierrot, C. Reynaud, A. Fournier: "DELTA: A Simple and Efficient Parallel Robot", Robotica, Vol.8, No.2, pp.105-109, 1990.

[15] F. Pierrot, A. Fournier and P. Dauchex: "Towards a Fully-Parallel 6 DOF Robot for High-Speed Applications", IEEE International Conference on Robotics and Automation, pp.1288-1293, 1991.

[16] Y. Takeda, H. Funabashi, H. Ichimaru: "Development of Spatial In-Parallel Actuated Manipulators with Six Degrees of Freedom with High Motion Transmissibility", JSME International Journal Series C: Mechanical Systems, Machine Elements and Manufacturing, Vol.40, No.2, pp.299-308.